

RSC Publishing Faraday Discussions

Carboxyl-functionalized nanochannels based on block copolymer hierarchical structures

Journal:	<i>Faraday Discussions</i>
Manuscript ID	FD-ART-02-2018-000015.R1
Article Type:	Paper
Date Submitted by the Author:	05-Mar-2018
Complete List of Authors:	Musteata, Valentina; King Abdullah University of Science and Technology Chisca, Stefan; King Abdullah University of Science and Technology (KAUST), Water Desalination and Reuse Center Meneau, Florian; LNLS Smilgies, Detlef; Cornell University, CHESS Nunes, Suzana; King Abdullah University of Science and Technology, Water Desalination and Reuse Center

SCHOLARONE™
Manuscripts

Carboxyl-functionalized nanochannels based on block copolymer hierarchical structures

Valentina-Elena Musteata^a, Stefan Chisca^a, Florian Meneau^b, Detlef-M. Smilgies^c, Suzana P. Nunes^{a*}

^aKing Abdullah University of Science and Technology (KAUST),
Biological and Environmental Science and Engineering (BESE) Division, 23955-6900 Thuwal, Saudi Arabia

^bBrazilian Synchrotron Light Laboratory (LNLS), SAXS1 Beamline, Rua Giuseppe Máximo Scolfaro,
13083-970 Campinas, São Paulo, Brazil

^cCornell High Energy Synchrotron Source (CHESS), Wilson Laboratory Cornell University, Ithaca, NY 14853, USA

When building artificial nanochannels having a scalable robust platform with controlled morphology is an important step, as well final functionalization of the channels for the selective transport of water and proteins. We have previously developed asymmetric membranes that has a surface layer of very sharp pore size distribution, surface charge and pore functionalization. Here a more complex bioinspired platform is reported. Hierarchical isotropic porous structures with spherical micrometer-sized cavities, interconnected by hexagonally ordered nanochannels, were prepared based on the phase separation of polystyrene-*b*-poly (t-butyl acrylate) block copolymers, following a nucleation and growth mechanism. The structure was imaged by scanning electron microscopy, demonstrating a high density of ordered nanochannels. The hexagonal order formed by the self-assembly in solution was confirmed by small angle x-ray scattering. The structure evolution was investigated by time-resolved grazing incident small angle x-ray scattering. The assembled hydrophobic hierarchical structure was then converted to hydrophilic by acid hydrolysis, leading to nanochannels covered by carboxylic groups and therefore convenient for water transport.

Introduction

Biological structures have been the ultimate model for preparation of synthetic porous materials, aiming at selective separations or scaffolds for biomedical applications. The morphology and functionality of biological channels have long fascinated membrane scientists.^{1, 2} Morphologies with exceptional regularity can be seen in simple unicellular biological systems such as diatoms. Mimicking the isoporosity and order of those systems would lead to much better size selective polymeric membranes, than those currently commercially available. Much more challenging is mimicking the functionality of protein channels and biological membranes, which are able to transport water with extreme selectivity as in the case of aquaporin or act as gate keepers for specific ions or small organic molecules. Bioinspired membranes are being manufactured by two main approaches. Many groups have focused on the incorporation of aquaporin into vesicles or as part of synthetic polymer films^{3, 4}, expecting to reach separation performances comparable to those observed in biological systems. Required steps are the protein expression and incorporation into a stabilizing support with suitable adhesion and compatibility and stability. The other approach is the design of completely artificial systems using organic polymers and functional groups. There are different hurdles to be overcome, but we believe that this is the most promising and sustainable route in the long term. A main challenge is the morphology control and preparation of well-defined nanochannels with different dimensions to serve size-driven separations. The other important tasks are the hydrophobicity/hydrophilicity control and the integration of active functionalization, which would give specific chemical selectivity and gate stimuli response. Interesting examples of the generation of artificial nanochannels have been reported, based on imidazole quartet and G-quadruplex assembly^{5, 6}, pillar[n]arenes⁷, crown ether stacking^{8, 9} and polypeptides¹⁰. Integrating the achievements in functional artificial nanochannels into robust membranes with long-range order and with the perspective of applications for separations in a reasonable scale is again not an easy task.

The pore size distribution of commercial membranes prepared by phase inversion or melt and stretch methods is mostly broad. Achieving isoporosity could lead to breakthroughs in protein purification and in the separations of other solutes in the ultra or nanofiltration range, but manufacturing isoporous membranes by competitive industrial methods have not yet been implemented. The only commercial isoporous membranes are track-etched, mostly characterized by low porosity and the nanoporous ceramic ones, which are highly brittle. Other emerging methods are reported, but still without industrialization. Examples are the induction of breath figures¹¹, which mainly lay on humidity condensation on solutions of low polarity, and polyHipes¹², which combine emulsion and in-situ polymerization. We have been working on porous structure generation using amphiphilic block copolymers. There are different methods of pore formation using block copolymers^{13, 14}, for instance using casting and selective etching or dissolution¹⁵, reactive phase separation¹⁶ and 2D printing¹⁷. Most of the work we reported in the last decade^{14, 18, 19} uses non-solvent induced phase separation and copolymer self-assembly for pore formation. In great part our focus has been on the preparation of isoporous asymmetric membranes with pores in the ultrafiltration range (20 to 60 nm diameter). The copolymer self-assembly takes place in solution and is consolidated by exposure to a non-solvent. A

phase separation by spinodal decomposition is initiated leading to a structure with a gradient of pore size. Selective ordered pores constitute the upper layer with a thickness not higher than 400 nm, supported on a rather disordered rougher pore structure. The membranes have been mainly prepared using polystyrene block copolymers with poly(4-vinyl pyridine), poly(ethylene glycol) or poly(acrylic acid). Their highly amphiphilic character facilitates the self-assembly in different geometries. Membranes prepared by this method with pores smaller than 5 nm in the nanofiltration range are rare and could be obtained by blending polystyrene-*b*-poly(4-vinyl pyridine) block copolymers with low molecular weight polystyrene-*b*-acrylic acid, which have acid-base interactions²⁰. The separations with this class of membranes is mainly based on size and surface charge. More recently two different systems have been investigated, which add specific functionalizations to the selective artificial nanochannels, allowing separations which are not strictly based on size difference. Membranes were formed by casting polystyrene-*b*-hydroxy polystyrene solutions²¹ with imidazole or pyridine, which particularly promotes hydrogen bond formation in the constrained nanopores for facilitated protein separation. In this case, lysozyme (14 kg/mol) could be preferentially transported, while poly(ethylene glycol) with lower molecular weight (10 kg/mol) was rejected. In another approach polybutadiene nanochannels were prepared from polystyrene-*b*-polybutadiene-*b*-polystyrene copolymers²², which were then photomodified by a thiol/diene reaction, creating hydrophilic channels for water transport.

The block copolymer membranes we previously developed in our group are highly asymmetric. In this work, we report a new method for preparing isotropic hierarchical structures, characterized by densely packed spherical cavities of micrometer diameter, which are highly interconnected by nanochannels. We believe these structures could be an excellent platform for bioinspired devices, which requires selective transport, storage of pharmaceutical active molecules or as biomedical scaffolds.

Methods

Materials. Polystyrene-*block*-poly(*t*-butyl acrylate) (PS-*b*-PtBA) copolymer with PS and PtBA molecular weights 66 kg/mol and 32 kg/mol, respectively, were purchased from Polymer Source, Inc. The polydispersity was 1.05. Tetrahydrofuran (THF), 1,4-dioxane (DOX), *N,N'*-dimethylformamide (DMF) and β -cyclodextrin (β -CD) were purchased from Sigma Aldrich. Trifluoroacetic acid (TFA) was provided by Fisher. All chemicals were used as received.

Preparation of hierarchical porous structures. 20 to 26 wt% PS-*b*-PtBA block copolymer were dissolved in DMF or in 1:3 THF/DMF or DOX/DMF mixtures. A 200 μ m solution layer was cast on a glass plate, the solvent was let to evaporate for 10 s to 10 min and the system was then immersed in water. In part of the work 6% β -CD with respect to the block copolymer was used as an additive.

Hydrolysis. After the porous structure formation, the PS-*b*-PtBA film was immersed in a TFA solution, stirred at room temperature for 24 h and washed with water. The hydrolysis was confirmed by Nuclear Magnetic Resonance (NMR) Spectroscopy on a Bruker Advance III 400 equipment, after dissolving in DMF-*d*₇.

Morphological characterization. The equilibrium morphology of PS-*b*-PtBA films was analyzed by transmission electron microscopy (TEM). The samples were annealed for 3 days at 110 °C under vacuum. The films were then embedded in the epoxy resin at 60 °C and then ultrathin sections (70 nm) were cut using an ultramicrotome (Leica EM UC6). The films were stained with ruthenium tetroxide (RuO₄) prior to imaging on a Tecnai (FEI company) microscope operating at 120 kV. RuO₄ preferentially stains the PS phase. The surface and cross-section of the porous films were imaged by scanning electron microscopy (SEM) on Nova Nano and Magellan microscopes, using an accelerating voltage of 2–5 kV, at a working distance of 1.5–5 mm. The samples were sputter coated with iridium or with platinum before imaging, using a Quorum Q150TES equipment.

Small Angle X-Ray Scattering (SAXS). The morphology of block copolymer dense annealed films and the order in solutions were analyzed at the SAXS1 beamline of the Brazilian Synchrotron facility (LNLS) at an energy of 8.0 keV. The X-ray wavelength was 0.155 nm, the distance between the sample and the detector was 3.057 m and area sampled by the beam was 1 mm². The sample was exposed during 600 s and the 2D scattering patterns were recorded by a Pilatus 300k detector with a pixel size of (172 μ m)². Plots of intensity versus scattering vector (*q*) were obtained by the radially integrated 2D patterns, after normalization to the intensity of primary beam and subtraction of background. Data fitting was performed using a sum of Lorenz functions by the Igor Pro 6.37 software.

Grazing-Incidence Small Angle Scattering (GISAXS). Time-resolved GISAXS experiments were performed at the D1 beam line of the Cornell High Energy Synchrotron Source. The beam had an energy of 10.6 keV and wavelength of 1.166 Å and the sample – detector distance was 1.77 m. GISAXS measurements with an incident angle of 0.13° were immediately initiated after casting the polymer solution with a doctor blading system.²³ 2D scattering patterns were acquired with Pilatus 200k detector using 3 and 4 s exposure time with 4 s pause between sample irradiation. Igor Pro 6.37 software was used to obtain 1 D profile of the scattered intensity versus scattering vector (*q*) for horizontal projections.

Results

The block copolymers chosen for this work, $PS_{66k}\text{-}b\text{-}PtBA_{32k}$, self-assemble when annealed above the glass transition temperatures of both blocks. The blocks thermodynamic characteristics are very similar. The dispersive, polar and hydrogen bonding Hansen solubility parameters²⁴ for PS are respectively $\delta_d= 18.5 \text{ MPa}^{1/2}$, $\delta_p= 4.5 \text{ MPa}^{1/2}$, $\delta_h= 2.9 \text{ MPa}^{1/2}$, while for PtBA are $\delta_d= 16 \text{ MPa}^{1/2}$, $\delta_p= 2.3 \text{ MPa}^{1/2}$, $\delta_h= 3.1 \text{ MPa}^{1/2}$. However, the Gibbs mixing energy is still high enough to drive demixing in equilibrium. After long annealing, a cylindrical hexagonal arrangement is achieved, as seen in Figure 1a. The PS blocks were preferentially stained with RuO_4 to emphasize the segregation. A Fourier Transform was applied to the TEM image and is shown as an inset, demonstrating the high order. The order was confirmed by SAXS. Figure 1b shows the repeating peaks at q equal to 1, $\sqrt{3}$, 2, $\sqrt{7}$, 3, characteristic of hexagonal order. The electron densities of PS and PtBA blocks are similar, $0.559 \text{ e}^{-1} \text{ mol/cm}^3$ and $0.546 \text{ e}^{-1} \text{ mol/cm}^3$, respectively. Therefore the scattering contrast is not high.

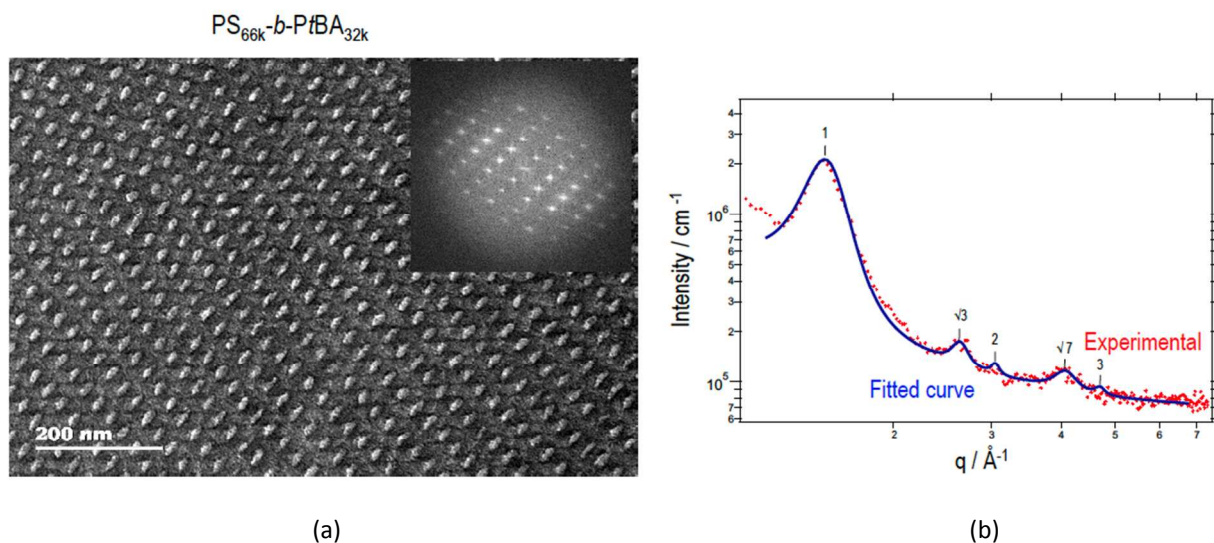


Figure 1. (a) TEM image of annealed $PS_{66k}\text{-}b\text{-}PtBA_{32k}$ samples sliced in an ultramicrotome and stained with RuO_4 ; (b) SAXS pattern for the same sample.

The polymer was dissolved in DMF and DMF mixtures with DOX or THF. The DMF/co-solvent ratio was kept at 3 to 1 weight. In all cases at high copolymer concentration (42 to 45 wt%) a relatively sharp peak was observed, indicating that order in solution is obtained in Figure 2a. The scattering system has d -spacings around 38.8-41.4 nm. Small secondary peaks indicate hexagonal order. The values of d -spacing are only slightly different in the 3 solvent mixtures, being higher in DOX/DMF. An increase was also observed with the addition of β -CD, which is known to strongly interact with the PtBA block.

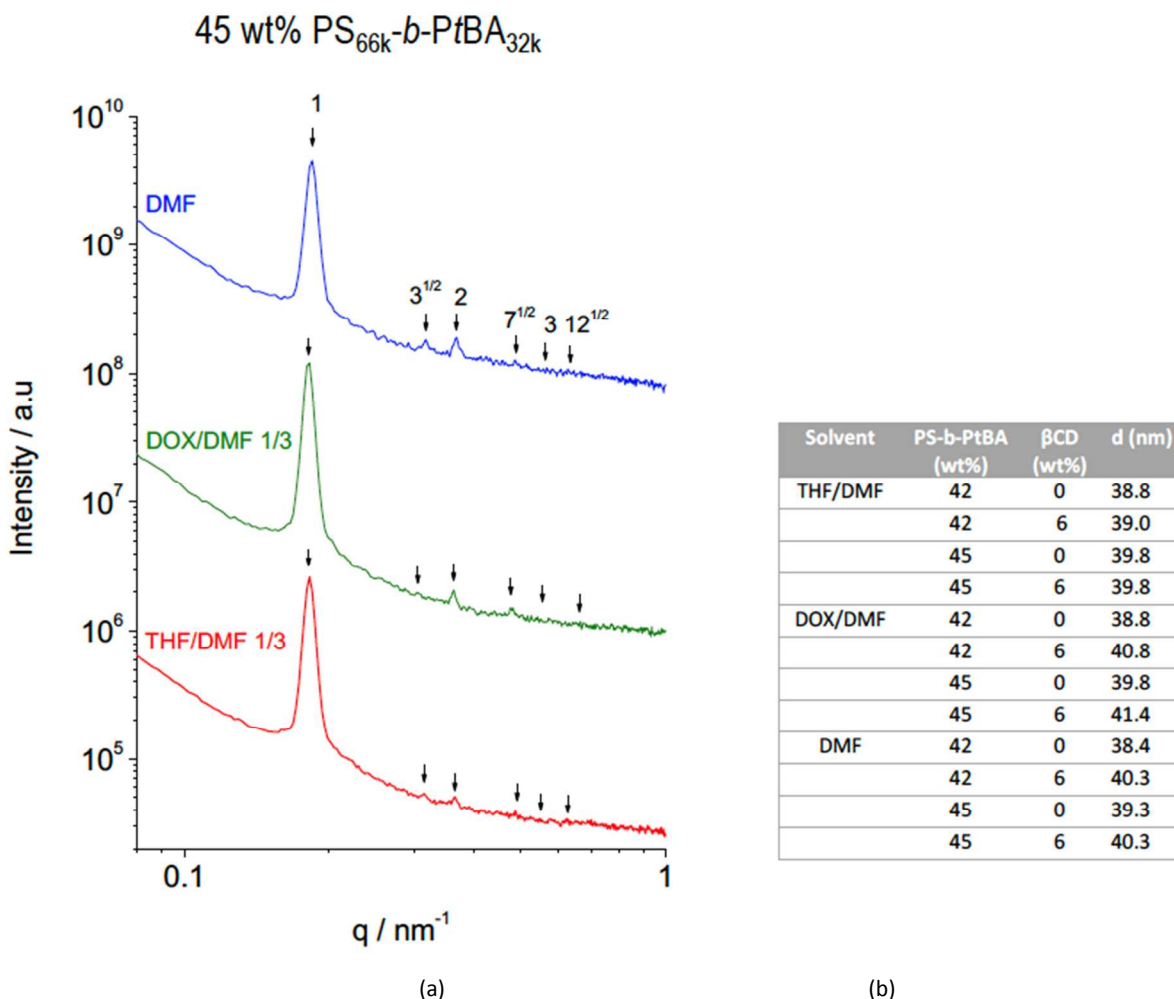


Figure 2. (a) SAXS patterns of 45wt% PS_{66k}-*b*-PtBA_{32k} solutions in DMF, 1:3 DOX/DMF and 1:3 THF/DMF mixtures; (b) d-spacing values, calculated based on q corresponding to the first peak, for solutions prepared with 42 or 45 wt% copolymer, with or without β CD. The β CD concentration is relative to the copolymer weight.

The solutions were cast, the solvent was partially evaporated during 1 to 10 minutes, the initiation of phase separation was indicated by the appearance of turbidity and the system was then immersed in water. A honeycomb morphology with spherical cavities homogeneously distributed across the film was observed for all investigated solutions, as demonstrated for a system cast from a solution in DMF. The cavities have diameters around 1.5 μm . The walls of each cavity are constituted by hexagonally arranged nanochannels. The film surface skin is also formed by the densely packed nanochannels. This makes the micrometer-sized cavities highly interconnected. The nanochannels have a diameter of ca. 15 nm. The self-assembly in solution revealed in Figure 2 is believed to play an important role in the formation of the hierarchical structure. To understand the formation process, time-resolved GISAXS experiments were conducted. Solutions with different copolymer concentrations were cast. The GISAXS patterns were recorded as a function of time, as shown in Figure 4. A peak is clearly seen in all cases, practically at the same q range (0.2 nm⁻¹) observed in static SAXS experiments. As time evolves, the peak shifts to lower q values. The corresponding d-spacing ($d=2\pi/q$) shifts from 34 to 39 nm for 26 wt% solutions and 36 to 38.5 nm for 20 wt% solutions. By the addition of β -CD, to the 26 wt% solution, the d-spacing values shift from 33 to 38 nm and remain constant after 300 s (Figure 4d). This indicates that, by adding β -CD and evaporating 5 min, the system achieves the equilibrium. The distance between nanochannel centers in the final solid structure is around 40 nm, as observed by SEM in Figure 3. The full width at half maximum was plotted for 20 wt% solutions as a function of time. A minimum is seen at 200 s, indicating that this is the time corresponding to the best order in this case. For solutions of higher concentration the peak sharpness continues to increase after 200 s, indicating that the best order requires longer time.

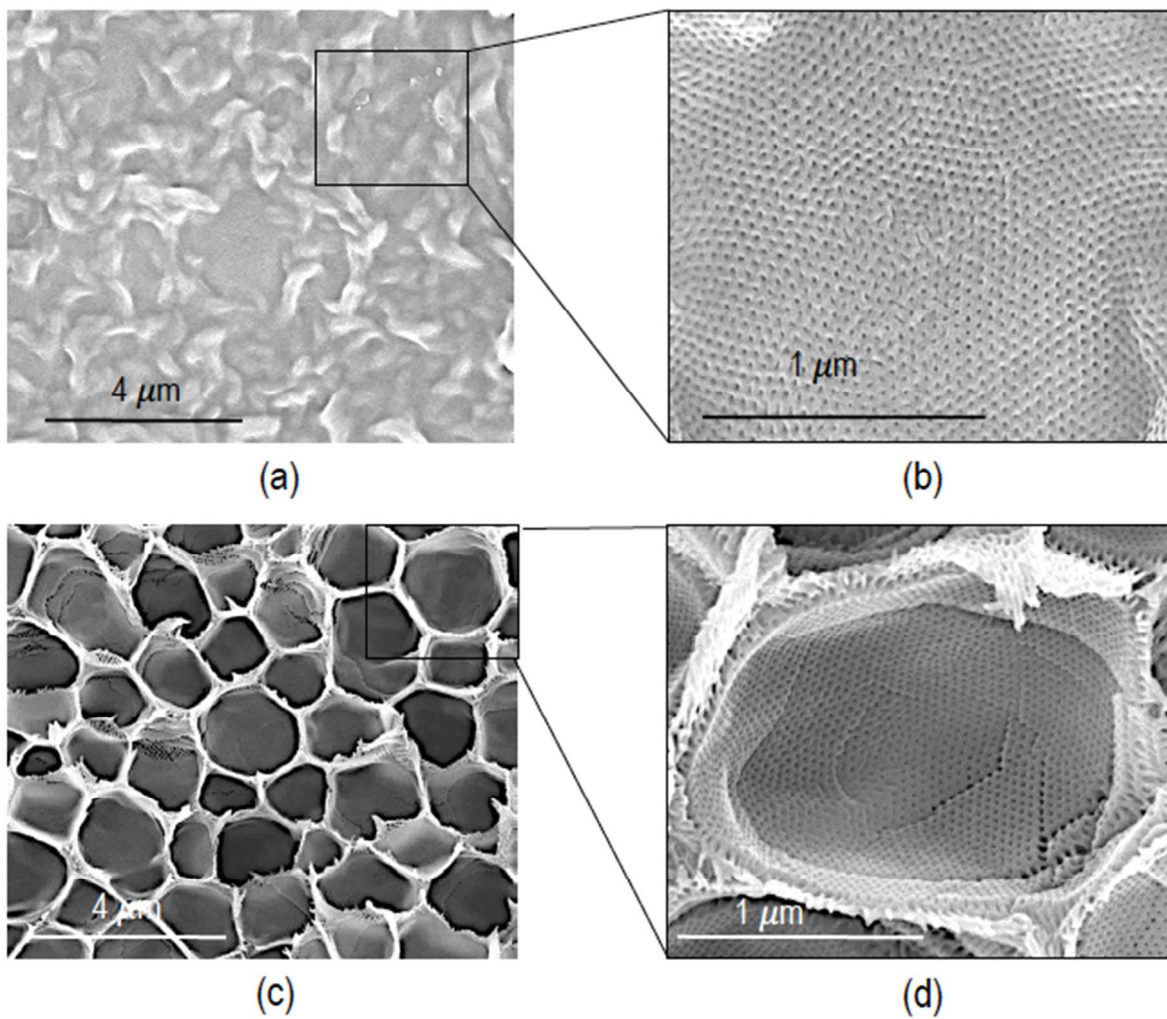


Figure 3. (a, b) Surface and (c, d) cross section images of isotropic porous films prepared by casting a 20 wt % PS_{66k}-*b*-PtBA_{32k} solution in DMF, followed by 5 minutes solvent evaporation and immersion in water.

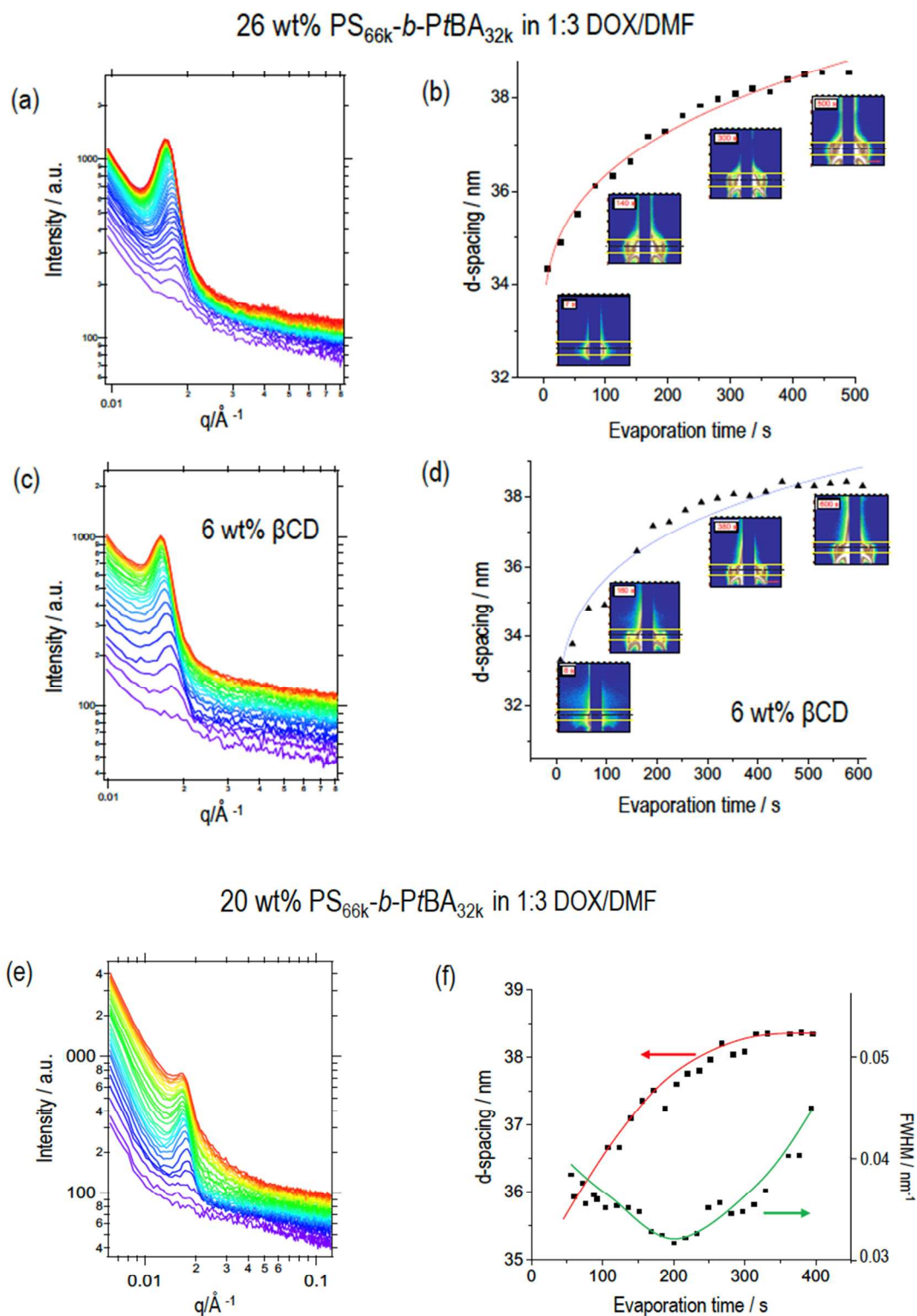


Figure 4. (a, c, e) Time-resolved GISAXS patterns of incipient hierarchically porous films, cast from (a, c) 26 wt% and (e) 20 wt% PS_{66k}-*b*-PtBA_{32k} solutions in 1:3 DOX/DMF, (c) with or (a, e) without addition of 6 wt% β CD; (b, d, f) plots of d-spacing as a function of evaporation time; (f) plot of full width at half maximum (FWHM) value for plot (e).

The nanochannels formation is guided by the copolymer self-assembly in solution. The mechanism is however quite different than that proposed for asymmetric block copolymer membranes, where ordered isopores are formed only on a single upper thin layer. There is a fundamental difference also between the morphologies illustrated in Figure 3b and 3d and the equilibrium one shown in Figure 1, which requires days of annealing to be reached. The hierarchical structures reported here are consolidated in less than a few minutes. We believe that the nanochannels formation is strongly linked to the formation of the large spherical cavities. The cavities are very probably the result of nucleation and growth (NG) of copolymer lean domains. The solvents used in this work are mainly DMF or DMF rich mixtures, which are highly polar. The Hansen solubility parameter polar and H-bond contributions are respectively 13.7 and 11.3 MPa^{1/2}. DMF is therefore a relatively poor solvent for PS_{66k}-*b*-PtBA_{32k}. Minor composition changes in terms of copolymer concentration by solvent evaporation, or humidity incorporation could initiate the phase separation. DMF evaporation is slow. It is possible that the system remains in a metastable condition, before proceeding with demixing. NG would lead to the evolution of initially isolated spherical domains. As they grow, the nuclei are constantly fed with a solution rich in DMF and diluted in the polymer. The matrix becomes highly concentrated in the polymer, forming thin walls separating the growing nuclei. The block copolymer molecules find themselves concentrated in a confined layer with dynamic solvent transport, orthogonally to the interfaces. Self-assembly is then induced, leading to the nanochannels formation. Self-assembly under confinement can lead to morphologies, which are hardly obtained in bulk. As the copolymer concentration continues to increase, gelation immobilizes the structure. By immersion in water, the solvent is extracted, the hierarchical structure is then fully solidified. Previous investigations of NG by light scattering report that logarithmic plots of the scattered intensity (*I*) and time lead to a straight line, whose slope is a measure of the NG kinetics²⁵⁻²⁷. Plots of intensity as a function of *q* do not have a maximum, in the opposite of systems following spinodal decomposition. The maxima in Figure 4a are in a range correlated to the self-assembly of the block copolymer in the nanoscale. They do not correspond to the macrophase separation. In the system investigated here two events are taking place in different scales: NG at a micrometer scale (possibly detectable at low *q* values) and copolymer self-assembly in a nanoscale (detectable at *q* near 0.2 nm⁻¹). In Figure 5 we plot log *I* vs log *t* at a fixed *q* = 0.08 nm⁻¹, which is below the range reflecting the self-assembly maximum. The concentration in Figure 5a is the same used to prepare the structures in Figure 3 and in that case a time of 300s was waited before immersion in water. For the 20 wt% solution, the NG process might start between 100 and 200s, when the slope becomes steeper. The addition of β-CD clearly influences the kinetics and a steeper slope was observed. When a higher initial concentration (26 wt%) was used (Figure 5b), matching the results of Figure 4, the kinetics is slower, due to the higher solution viscosity. The slope is decreased above 200s, in systems without β-CD. This is an indication of reaching the gelation condition. The concomitant self-assembly seen in Figure 4b slowly stabilizes with *d*-spacing just above 38 nm.

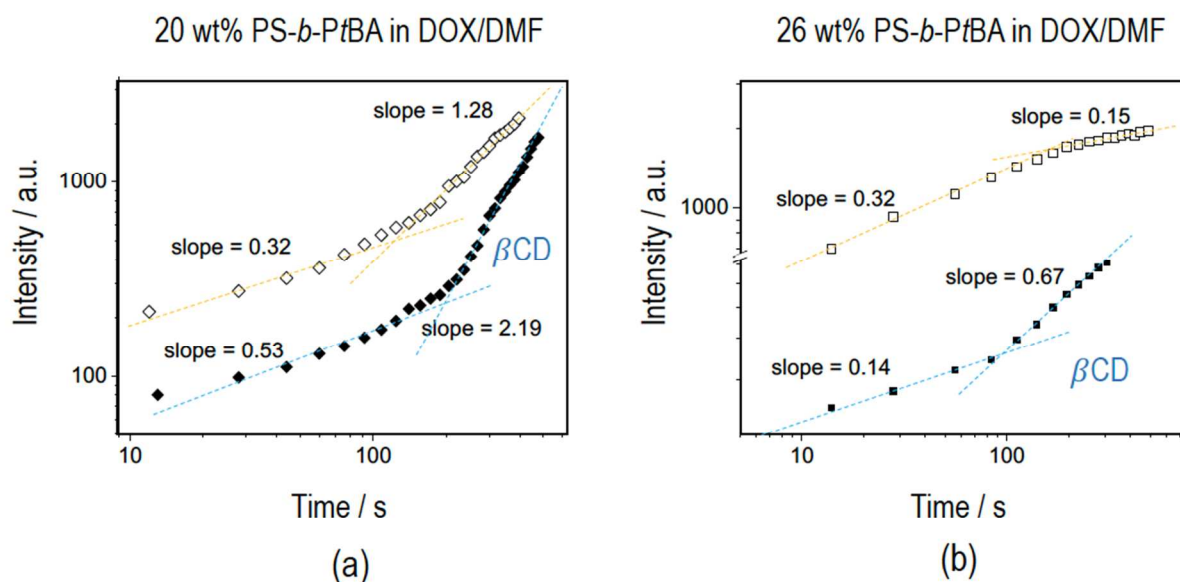


Figure 5. GISAXS scattering intensity as a function of time for (a) 20 and (b) 26 wt% PS_{66k}-*b*-PtBA_{32k} solutions in 1:3 DOX/DMF cast with or without β-CD. The intensity values were taken at *q* = 0.08 nm⁻¹.

The obtained hierarchical structure provides the large cavities, which could be used for instance as liquid storage. The cavities in a dry film reduce weight and reduce the resistance to transport. The structure combines multilayers of nanopores multiplying their action in terms of selectivity or interactions with the pore walls. The overall mechanical stability of the system is expected to be much higher than in the case of having only a single porous self-standing layer.

If the nanochannels are aimed for transport, their chemistry is as important as their size. PS-*b*-PtBA is hydrophobic. An important step in this work was the conversion of the pre-formed structures into hydrophilic carboxylic covered systems, by promoting the acid hydrolysis, through reacting with TFA. PS-*b*-poly(acrylic acid) (PS-*b*-PAA) is then obtained.

The final hydrolyzed structure is shown in Figure 6, imaged by SEM. The nanochannels between cavities are clearly seen. The SAXS analysis of the solid dry structure confirms that highly ordered pores are present. The scattering profile presents multiple reflections, which is rarely met for asymmetric nanoporous polymeric membranes. This points out the presence of a high density of regular pores. Still, the higher order reflections peaks are quite overlapped. To accurately estimate the peak positions and to assign a structure to the scattering profile, data deconvolution was performed using Igor Pro 6.37 software.²⁸ The best fitting (lowest residuals) was obtained when five Lorentz functions were used to describe the scattering profile (Figure 6a). The relative positions of the peaks are q/q^* : 1, 1.73, 2.02, 2.64, 3.47, very close to $1, \sqrt{3}, \sqrt{4}, \sqrt{7}, \sqrt{12}$, which are characteristic of hexagonally packed cylinders, with domain spacing of 38.95 nm. The presence of the higher order reflections in the scattering profile and the small value of full width at half maximum value (0.037 nm^{-1}) for the primary peak confirmed a very good long-range order.

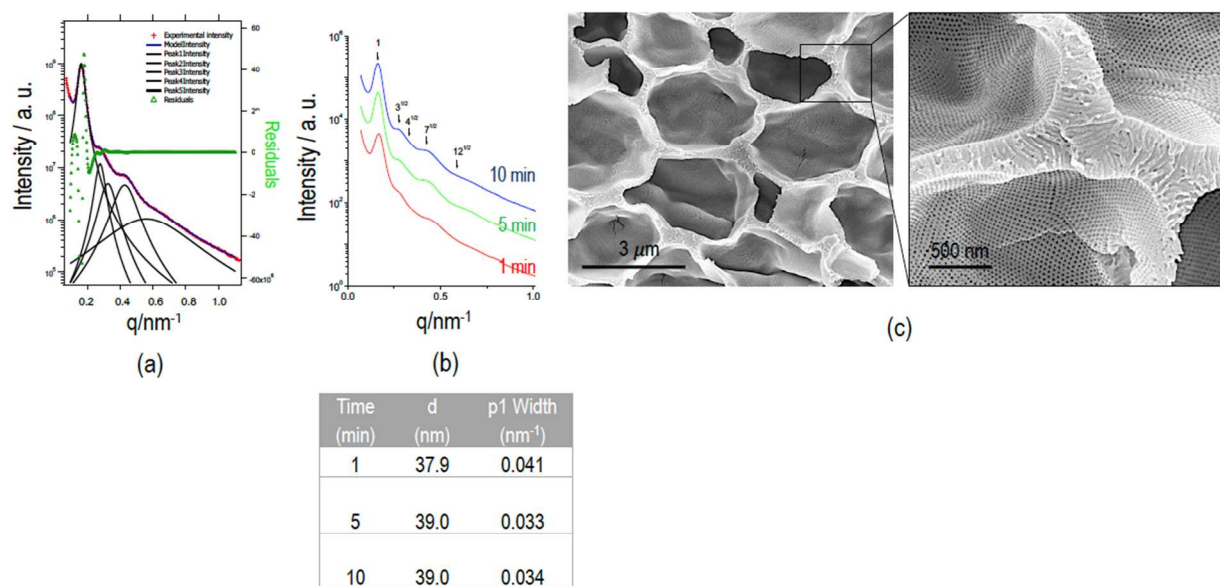


Figure 6. (a, b) SAXS patterns of hierarchical and isotropic porous films prepared by casting of 20 wt% PS_{66k}-*b*-PtBA_{32k} solutions in DMF, followed by hydrolysis; the curves in (b) were obtained from experimental scattering values fitted as exemplified in (a); (c) SEM cross sectional images of films prepared with 5 minutes evaporation, followed by hydrolysis. The table shows d-spacing and the full width at half maximum value for different evaporation times.

A completely different structure is obtained if the hydrolysis is performed in a first step and the resulting PS-*b*-PAA is solubilized in 1:3 DOX/DMF, cast and immersed in water. Figure 7 shows that a completely different structure is achieved, without nanochannels.

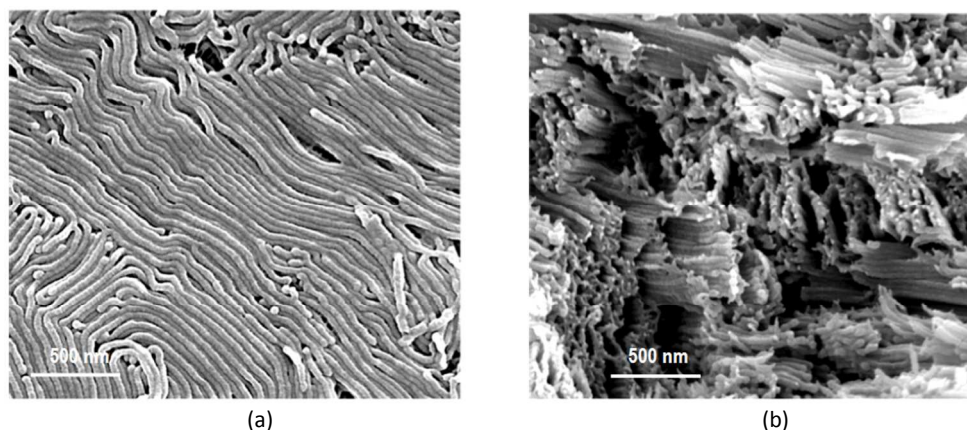


Figure 7. Asymmetric porous membranes cast from PS-*b*-PAA (hydrolyzed PS-*b*-PtBA) solutions in 1:3 DOX/DMF, evaporated for 5 min and immersed in water: (a) surface and (b) cross-sectional SEM images.

Conclusions

A new isotropic hierarchical structure containing micrometer-sized regular cavities connected by hexagonally ordered nanochannels was prepared. The formation is proposed to occur due to the co-occurrence of nucleation and growth of copolymer lean phases, block copolymer self-assembly in the confined space between nuclei, under the influence of the solvent transfer to the growing nuclei and finally gelation. The observations were supported by morphological investigation and time-resolved GISAXS experiments. The hydrophilicity was added to the system by conversion of the PtBA blocks to carboxylic groups. A multi-layered system with carboxyl-functionalized nanochannels has been generated, intercalated by larger cavities, which is expected to contribute to low resistance to transport.

Conflicts of interest

There are no conflicts to declare.

Acknowledgements

The authors acknowledge Cornell High Energy Synchrotron Source (CHESS) in USA and Laboratório Nacional de Luz Síncrotron (LNLS) in Brazil for the access to the GISAXS and SAXS synchrotron facilities and the support at the beamline. CHESS was supported by the National Science Foundation and the National Institutes of Health/National Institute of General Medical Sciences under NSF award DMR-1332208.

References

1. H. Zhang, Y. Tian and L. Jiang, *Nano Today*, 2016, **11**, 61-81.
2. X.-Y. Yang, L.-H. Chen, Y. Li, J. C. Rooke, C. Sanchez and B.-L. Su, *Chemical Society Reviews*, 2017, **46**, 481-558.
3. C. Tang, Y. Zhao, R. Wang, C. Hélix-Nielsen and A. Fane, *Desalination*, 2013, **308**, 34-40.
4. H. Wang, T. S. Chung, Y. W. Tong, K. Jeyaseelan, A. Armugam, Z. Chen, M. Hong and W. Meier, *small*, 2012, **8**, 1185-1190.
5. Y. Le Duc, M. Michau, A. Gilles, V. Gence, Y. M. Legrand, A. van der Lee, S. Tingry and M. Barboiu, *Angewandte Chemie International Edition*, 2011, **50**, 11366-11372.
6. M. S. Kaucher, W. A. Harrell and J. T. Davis, *Journal of the American Chemical Society*, 2006, **128**, 38-39.
7. Y.-x. Shen, P. O. Saboe, I. T. Sines, M. Erbakan and M. Kumar, *Journal of Membrane Science*, 2014, **454**, 359-381.
8. M. Barboiu, S. Cerneaux, A. van der Lee and G. Vaughan, *Journal of the American Chemical Society*, 2004, **126**, 3545-3550.
9. T. M. Fyles, *Chemical Society Reviews*, 2007, **36**, 335-347.
10. S. Litvinchuk, N. Sordé and S. Matile, *Journal of the American Chemical Society*, 2005, **127**, 9316-9317.
11. A. Munoz-Bonilla, M. Fernández-García and J. Rodríguez-Hernandez, *Progress in Polymer Science*, 2014, **39**, 510-554.
12. M. S. Silverstein, *Progress in Polymer Science*, 2014, **39**, 199-234.

13. S. P. Nunes and A. Car, *Industrial & Engineering Chemistry Research*, 2012, **52**, 993-1003.
14. S. P. Nunes, *Macromolecules*, 2016, **49**, 2905-2916.
15. W. A. Phillip, B. O'Neill, M. Rodwogin, M. A. Hillmyer and E. Cussler, *ACS applied materials & interfaces*, 2010, **2**, 847-853.
16. E. A. Jackson and M. A. Hillmyer, *ACS nano*, 2010, **4**, 3548-3553.
17. S. Qu, Y. Shi, S. Benavides, A. Hunter, H. Gao and W. A. Phillip, *Chemistry of Materials*, 2017, **29**, 762-772.
18. M. Karunakaran, S. P. Nunes, X. Qiu, H. Yu and K.-V. Peinemann, *Journal of Membrane Science*, 2014, **453**, 471-477.
19. P. Madhavan, K.-V. Peinemann and S. P. Nunes, *ACS applied materials & interfaces*, 2013, **5**, 7152-7159.
20. H. Yu, X. Qiu, N. Moreno, Z. Ma, V. M. Calo, S. P. Nunes and K. V. Peinemann, *Angewandte Chemie International Edition*, 2015, **54**, 13937-13941.
21. B. Sutisna, G. Polymeropoulos, E. Mygiakis, V. Musteata, K.-V. Peinemann, D.-M. Smilgies, N. Hadjichristidis and S. P. Nunes, *Polymer Chemistry*, 2016, **7**, 6189-6201.
22. B. Sutisna, G. Polymeropoulos, V. Musteata, R. Sougrat, D. M. Smilgies, K. V. Peinemann, N. Hadjichristidis and S. P. Nunes, *Small*, 2017.
23. D. M. Smilgies, R. Li, G. Giri, K. W. Chou, Y. Diao, Z. Bao and A. Amassian, *physica status solidi (RRL)-Rapid Research Letters*, 2013, **7**, 177-179.
24. C. M. Hansen, *Hansen solubility parameters: a user's handbook*, CRC press, 2007.
25. K.-V. Peinemann, J. Maggioni and S. Nunes, *Polymer*, 1998, **39**, 3411-3416.
26. S. P. Nunes and T. Inoue, *Journal of membrane science*, 1996, **111**, 93-103.
27. J. Wijmans, H. Rutten and C. Smolders, *Journal of Polymer Science Part B: Polymer Physics*, 1985, **23**, 1941-1955.
28. J. Ilavsky and P. R. Jemian, *Journal of Applied Crystallography*, 2009, **42**, 347-353.